Journal Pre-proof

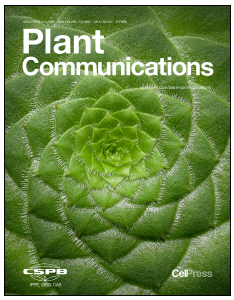

A chromosome-level, haplotype-phased genome assembly for *Vanilla planifolia* highlights that partial endoreplication challenges accurate whole genome assembly

Q. Piet, G. Droc, W. Marande, G. Sarah, S. Bocs, C. Klopp, M. Bourge, S. Siljak-Yakovlev, O. Bouchez, C. Lopez-Roques, S. Lepers-Andrzejewski, L. Bourgois, J. Zucca, M. Dron, P. Besse, M. Grisoni, C. Jourda, C. Charron

PII: S2590-3462(22)00080-3

DOI: https://doi.org/10.1016/j.xplc.2022.100330

Reference: XPLC 100330

To appear in: *PLANT COMMUNICATIONS*

Received Date: 30 October 2021

Revised Date: 10 April 2022

Accepted Date: 27 April 2022

Please cite this article as: Piet, Q., Droc, G., Marande, W., Sarah, G., Bocs, S., Klopp, C., Bourge, M., Siljak-Yakovlev, S., Bouchez, O., Lopez-Roques, C., Lepers-Andrzejewski, S., Bourgois, L., Zucca, J., Dron, M., Besse, P., Grisoni, M., Jourda, C., Charron, C., A chromosome-level, haplotype-phased genome assembly for *Vanilla planifolia* highlights that partial endoreplication challenges accurate whole genome assembly, *PLANT COMMUNICATIONS* (2022), doi: https://doi.org/10.1016/j.xplc.2022.100330.

A chromosome-level, haplotype-phased genome assembly for *Vanilla planifolia* highlights that partial endoreplication challenges accurate whole genome assembly

Piet Q.[1,*], Droc G. [2,3,4,*,#], Marande W.[5,*], Sarah G.[6,*], Bocs S.[2,3,4,*], Klopp C.[7,*], Bourge M.[8], Siljak-Yakovlev S.[9], Bouchez O.[10], Lopez-Roques C.[10], Lepers-Andrzejewski S.[11], Bourgois L.[12], Zucca J.[13], Dron M.[14], Besse P.[15], Grisoni M.[16#], Jourda C.[1,#] and Charron C.[1,*]

[1]*CIRAD, UMR PVBMT, F-97410 Saint-Pierre, La Réunion, France.*

[2]*CIRAD, UMR AGAP Institut, F-34398 Montpellier, France.*

[3]*UMR AGAP Institut, Univ Montpellier, CIRAD, INRAE, Institut Agro, F-34398 Montpellier, France.*

[4]*French Institute of Bioinformatics (IFB) - South Green Bioinformatics Platform, Bioversity, CIRAD, INRAE, IRD, F-34398 Montpellier France.*

[5]*INRAE, CNRGV, Genotoul, 31326 Castanet-Tolosan, France.*

[6]*AGAP, Univ. Montpellier, CIRAD, INRAE, Montpellier SupAgro, Montpellier, France.*

[7]*Plateforme Bioinformatique, Genotoul, BioinfoMics, UR875 Biométrie et Intelligence Artificielle, INRAE, Castanet-Tolosan, France*

[8]*Cytometry Facility, Imagerie-Gif, Université Paris-Saclay, CEA, CNRS, Institute for Integrative Biology of the Cell (I2BC), 91198, Gif-sur-Yvette, France.*

[9]*Université Paris-Saclay, Ecologie Systématique Evolution, Univ. Paris-Sud, CNRS, AgroParisTech, Université Paris-Saclay, Orsay Cedex, France.*

[10]*INRAE, GeT-PlaGe, Genotoul, 31326, Castanet-Tolosan, France.*

[11]*Etablissement Vanille de Tahiti, Uturoa, French Polynesia, France.*

[12]*Eurovanille, Rue de Maresquel, 62870 Gouy Saint André, France.*

[13]*V. Mane Fils, Département Biotechnologie, 06620 Le Bar Sur Loup, France.*

[14]*Université Paris-Saclay, CNRS, INRAE, Univ Evry, Institute of Plant Sciences Paris-Saclay (IPS2), 91405 Orsay, France.*

[15]*Université de la Réunion, UMR PVBMT, Saint-Pierre, La Réunion, France.*

[16]*CIRAD, UMR PVBMT, 501 Tamatave, Madagascar.*

* These authors contributed equally to this work

[#]Correspondance : michel.grisoni@cirad.fr ; cyril.jourda@cirad.fr ; gaetan.droc@cirad.fr

SHORT SUMMARY

The genome of the orchid *Vanilla planifolia* (4.09 Gb, 16 pairs of chromosomes) is very prone to partial endoreplication (PE) which leads to a very unbalanced DNA content in the cells. We report here first molecular evidence of PE at chromosome scale through the assembly and annotation of an accurate haplotype-phased genome of *V. planifolia*. Distinct haplotype-specific sequencing depth variation patterns suggest complex molecular regulation of endoreplication along chromosomes. To facilitate post-genomics efforts, an integrated public and user-friendly web portal (the Vanilla Genome Hub) has been developed.

KEYWORDS

Vanilla, Whole genome sequencing, Optical mapping, Strict partial endoreplication, Genome Hub

ABSTRACT

Vanilla planifolia, the species cultivated to produce one of the world's most popular flavors, is highly prone to partial genome endoreplication (PE) which leads to highly unbalanced DNA content in cells. We report here first molecular evidence of PE at chromosome scale by the assembly and annotation of an accurate haplotype-phased genome of *V. planifolia*. Cytogenetic data demonstrated that the diploid genome size is 4.09 Gb, with 16 chromosome pairs although aneuploid cells are frequently observed. Using PacBio HiFi and optical mapping, we assembled and phased a diploid genome of 3.4 Gb with a scaffold N50 of 1.2 Mb and 59,128 predicted protein-coding genes. The atypical k-mers frequencies and the uneven sequencing depth observed agreed with our expectation of unbalanced genome representation. Sixty-seven percent of the genes were scattered over only 30% of the genome, putatively linking gene-rich regions and the endoreplication phenomenon. On the contrary, low coverage regions (non-endoreplicated) were rich in repeated elements but also contained 33% of the annotated genes. Furthermore, this assembly showed distinct haplotype-specific sequencing depth variation patterns suggesting a complex molecular regulation of endoreplication along the chromosomes. This high-quality anchored assembly represented 83% of the estimated *V. planifolia* genome.

It provides a significant step towards the elucidation of this complex genome. To support post-genomics efforts, we developed the Vanilla Genome Hub, a user-friendly integrated web portal that allows centralized access to high-throughput genomic and other omics data, and interoperable use of bioinformatics tools.

INTRODUCTION

Endoreplication, characterized by a series of DNA replications in the nucleus without mitotic cell division, is found in a large number of both animal and plant species (Lee et al., 2009). During regular endoreplication, each step of this mechanism leads to a two-fold nuclear DNA content increase in somatic cells (2C to 4C, 8C, 16C, etc.), where 1C corresponds to the DNA content of the non-replicated holoploid chromosome set. Endoreplication is very common in plants and related to various biological processes, such as plant development and growth, and occurs in response to biotic and abiotic stresses (Bourdon et al., 2012; Lang and Schnittger, 2020). This phenomenon depends on the type of tissue and its stage of development, suggesting involvement in cell differentiation and maintenance of the final stage of differentiation (Bhosale et al., 2018). The molecular mechanisms involved in regular endoreplication have been particularly studied in *Arabidopsis thaliana* over the past few years. A downregulation of mitotic activity caused by mitotic Cyclin-dependent kinase (CDK)-cyclin complexes has been shown to be directly involved in the control of endoreplication (Lang and Schnittger, 2020).

In many orchid species, measurements of genomic content by flow cytometry (FCM) did not agree with the commonly accepted model of complete endoreplication. In this case, nuclear DNA content in endoreplicated cells was present at less than two-fold the 2C cells content. Since this ratio was constant, whatever the cell ploidy level, for a given *Vanilla* species, it was suggested that the nuclear DNA could be categorized into two parts: The P fraction, subject to endoreplication, and the F fraction, not endoreplicated (Brown et al., 2017). These fractions are constant in all cells undergoing PE, which suggests fine regulations of genome rearrangements. The fact that the gametes are haploid also suggests the presence of molecular mechanisms allowing the isolation of the holoploid genome. This type of endoreplication, that appears to be specific to the Orchidaceae lineage in plants has been successively termed "progressively partial endoreplication (PPE) (Bory et al. 2008; Trávníček et al., 2015; Hřibová et al., 2016), strict partial endoreplication (SPE) (Brown et al., 2017), and more recently

"partial endoreplication (PE) (Chumová et. al, 2021; Trávníček et al., 2021). To be in line with the latest works and in order to harmonize the terminology of this phenomenon, the term PE will be used in this work. So far, PE has been observed in all species studied within the genus *Vanilla* (Bory et al., 2008; Brown et al., 2017; Lepers-Andrzejewski et al., 2011; Trávníček et al., 2015).

Vanilla planifolia G. Jackson is an emblematic orchid cultivated for fruit (pod) fragrance. Pods contain many aromatic compounds, particularly vanillin in high proportion (Perez-Silva et al., 2006). In this species, diploid nuclei (2C) are mainly found in nodal tissues (with PE up to 32E) while the nuclei of mature leaf cells contain low 2C fraction and PE up to 64E (Brown *et al.*, 2017). The F fraction was estimated to be 71.6% of the genome while the P fraction (28.4%) could be duplicated up to 64E. In addition, the proportion of the non-endoreplicated (F) genome varies greatly from species to species. It is very high in *V. pompona* (F=81%) but rather low in *V. mexicana* (F=17%) (Brown *et al.*, 2017). Several studies on orchids have also shown that species prone to PE have a larger genome than those prone to conventional endoreplication (Chumová et al., 2021; Trávníček et al., 2019; Trávníček et al., 2015). Nevertheless, the molecular mechanisms involved in PE are not yet elucidated.

A chromosome-scaled, phased *V. planifolia* genome (Daphna cultivar) was recently reported, highlighting haplotype difference and one ancestral whole genome duplication shared by all sequenced orchids (Hasing et al., 2020). However, the 1.5 Gigabase (Gb) of the assembled genome was far from the *V. planifolia* genome size estimated to be about 4 Gb using FCM measurement (Bory *et al.*, 2008; Lepers-Andrzejewski *et al.*, 2011), which suggests a putative high incomplete genome assembly concerning Daphna. As mentioned by Hasing et al. (2020), the reason for the genome size discrepancy between flow cytometry and assembly results remained to be elucidated. With about 65% of the *V. planifolia* genome missing in Daphna assembly, we hypothetize that the missing part of the genome corresponds mainly to the F (non-endoreplicated) fraction (71.6%) (Brown *et al.*, 2017), due to its lower representation and therefore its lower sequencing depth.

Here we develop an approach combining FCM, cytogenetics and whole genome sequencing using most recently developed technologies (Supplemental Figure 1) and a 2C fraction enriched tissue (nodes), resulting in reduced P/F therefore greater proportion of the F fraction to unlock this issue. We demonstrate that size discrepancy was due to the occurrence of PE, for

which further knowledge at chromosome scale was gained from this study. We present the most complete version to date of a high-quality chromosome-level phased genome of *V. planifolia* using a traditional vanilla cultivar from the Indian Ocean region (CR0040). Our results are shared through a web portal facilitating data access, use and analyses by a wide community.

RESULTS

Genome size, ploidy level and chromosome content

The 2C genome size of *V. planifolia* CR0040, a traditional vanilla cultivar from La Reunion island (Supplemental Note 1), was estimated in nodal tissues to be 4.18 ± 0.08 pg by FCM (Supplemental Note 1), corresponding to 4.09 Gb (Doležel et al., 2003). To estimate PE levels, fluorescence ratio of DNA content between consecutive peaks of endoreplication levels was estimated (Supplemental Note 1; Supplemental Figure 2 and Supplemental Table 1). Results showed no significant difference (calculated t-value of 1.116, 1.900, 0.935, 0.365 compared to Student table t-value (α=0.05) of 2.131) between PE pattern of CR0040 and other *V. planifolia* cultivars such as CR1110 (2C = 4.16 ± 0.04 pg) studied by Brown et al. (2017). Replicated fraction P was also calculated (P = 30.5% ± 3.2). The equivalent amount 2p was then P x 2C = 1.275 pg, which meant that the absolute quantity p was 0.637 pg and the absolute quantity f of fixed amount was 1.453 pg (Figures 1A, 1B; Supplemental Note 1). The karyotype of *V. planifolia* obtained by cytogenetics approaches (Supplemental Note 1) appeared as of bimodal type, namely composed by 16 both large and small chromosome pairs (Figures 2A, 2B, 2C), although aneuploid cells were frequently observed, such as those with only 28 chromosomes (Figures 2D, 2E). *V. planifolia* chromosomes possess important portions of telomeric and pericentromeric heterochromatin which made the determination of their morphology difficult. In the interphase nuclei, this heterochromatin was present in the form of numerous chromocenters clearly visible both after staining with orcein (Figure 2F) and DAPI (Figure 2G). This type of heterochromatin is unspecific while the heterochromatin linked to rRNA genes is rich in G-C bases. Only one locus (two spots) of rDNA (18S-5.8S-26S) was present in the genome of *V. planifolia* (Figure 2H, arrows), evidenced after chromomycin (CMA3) staining. Our results also revealed, after Hoechst 33258 staining, that in the *V. planifolia*

chromosomes AT-rich DNA regions were more represented than those GC-rich and that some chromosomes were entirely or almost entirely heterochromatinized (Figure 2I).

Whole genome assembly and k-mers analysis

CR0040 genome sequencing produced 69 Gb Pacific Biosciences (PacBio) HiFi long-reads, 147 Gb Oxford Nanopore Technology (ONT) long-reads and 200 Gb Illumina 10X Genomics short-reads (Supplemental Note 1 and Supplemental Table 2). These DNAseq reads were assembled using different bioinformatics pipelines. The best result was obtained using only high quality HiFi long-reads (Supplemental Note 2 and Supplemental Tables 3 and 4). Contigs from HiFi reads assembly were scaffolded with optical maps to obtain a final phased assembly of 3.4 Gb (1.5 Gb for haplotype A and 1.9 Gb for haplotype B) representing around 83% of the expected genome size. One third of the assembly could be anchored onto 14 chromosomes using published Daphna chromosomes as references (Hasing *et al.*, 2020). Unfortunately, no data could help to organize the remaining contigs into the two missing chromosomes. Therefore, the remaining two thirds correspond to unanchored additional sequences that were compiled into two unknown random pseudomolecules A0 and B0. The final assembly comprised 24,534 contigs with a contig N50 length of 924 kb. The lengths of the 14 chromosomes ranged from 73.5 Mb (Chr01) to 20 Mb (Chr14). Main genome assembly statistics are synthesized in Table 1.

In order to understand how the PE affects the assembly, a k-mer analysis was produced. The results should reflect the sequencing coverage of the different genome fractions present in our raw data and assembly. Briefly, the reads were split into overlapping k-mers (47 mers in our case), then the k-mers were sorted and the occurrences counted. These counts were then used to produce a histogram. A spectra-cn plot was used to compare the k-mers found in the reads versus the k-mers found in the assembly (Supplemental Figure 3). The X-axis gives the number of times a given k-mer was found in all the reads, reflecting the coverage of the k-mer. The Y-axis gives a value representing the number of k-mers that were found a specified number of times (X-axis value). Interestingly, two k-mers distributions were centered at 42X and 84X, representing classical diploid distribution with the heterozygous and homozygous k-mer content. We assumed that these peaks represented the k-mers of the endoreplicated fraction with high sequencing depth due to higher representation. Remarkably, the graph also showed

an additional k-mers distribution centered around 10X (Supplemental Figure 3, red arrow). This distribution can easily be mistaken with the erroneous k-mers distribution but we assumed that it represented non-endoreplicated k-mers of the *V. planifolia* genome, with low-sequencing depth due to lower representation.

To validate the assembly and compare it with the already published reference, we produced four k-mers spectra-cn plots showing Daphna Illumina reads and CR0040 HiFi reads k-mer distributions colored both with Daphna and CR0040 assemblies (Figure 3). A spectra-cn plot enables to compare the k-mers found in the reads versus the k-mers found in the assembly. The k-mer histogram from reads is colored by the number of times each k-mer is found in the assembly. For a heterozygous diploid assembly, we expected to find two distributions, on the left hand the heterozygous distribution which should be colored in red because each k-mer is only found once in the assembly and on the right hand the homozygous distribution which is purple because the corresponding k-mers are found twice in the assembly. The black area at the far left of the diagram corresponds to k-mers including sequencing errors which are found a limited number of times in the reads and never in the assembly. Daphna Illumina sequencing being deeper resulted in a better separation between the homozygous (80X sequencing depth) and heterozygous (160X depth) k-mers fractions in the spectra-cn graph, compared to CR0040 (Figures 3A and 3B against 3C and 3D). The same pattern occurred for CR0040 HiFi data around 45X and 90X (Figure 3C). The differences between Figures 3A and 3C come from the sequencing depth and the type of tissue used: mature leaves with a higher proportion of the P fraction for Daphna and nodal tissues with a lower P/F ratio for CR0040. The k-mer distribution of the non-endoreplicated fraction (low coverage) were not found in the Daphna assembly (black area left of Figures 3B and 3D) but are mostly present in the CR0040 assembly. Regarding the completeness of the Daphna reference assembly, the spectra-cn plots (Figures 3B and 3D) showed that part of the heterozygous fraction was missing (orange arrows) and some k-mers were in over-represented copies (>2X) in both heterozygous and homozygous fractions (Figure 3B, black arrows). The spectra-cn diagram also showed heterozygous content present twice or more times instead of once in this assembly (Figure 3, black arrows) which could indicate spurious duplications. As a whole, our genome assembly of CR0040 is close in genome size to FCM estimation and has the expected k-mer diploid profile with a well-represented non-endoreplicated fraction (Figures 1C and 1D).

Genes and transposable elements annotation

The assembled genome supplemented with transcriptomic data from nine distinct tissues made it possible to identify 59,128 protein coding genes (26,392 for haplotype A and 32,736 for haplotype B) among which 90.31% could be associated with a function (Supplemental Note 3, Supplemental Tables 5 to 10). Sixty-seven percent of predicted genes were anchored onto the 14 chromosome pairs, and the remaining 33% onto the two random mosaic chromosomes that were constructed from the unanchored scaffolds and contigs (Figure 4A, blue distributions). We estimated the annotation completeness at 93.2% with the BUSCO (Benchmarking Universal Single-Copy Orthologs) approach using the Viridiplantae database. In total, 72% of the assembly consisted of repeats including single sequence repeats (SSR, 15.4%) and 9.7% other low complexity regions (Supplemental Note 3, Supplemental Table 11). High content of retrotransposons was found (41.5%), while content in DNA transposons was low (1.4%). The Long Terminal Repeats (LTR) retrotransposon content was richer in Gypsy (9.7%, Figure 4A, purple distributions) than in Copia (6.1%, Figure 4A, orange distribution), although a number of annotated retrotransposons (12.5%) were not more precisely classified. The two random mosaic chromosomes were enriched in repeats and showed low gene density and low sequencing depth (Figure 4A, green distributions and Supplemental Table 12). Indeed, compared to the 14 chromosome sequences, the unanchored regions showed higher proportions of Long Interspersed Nuclear Elements (LINEs) sequences (8% and 14.05%, respectively), and this for both haplotypes. On the contrary, DNA transposons (3.14% and 0.93%) as well as Short Interspersed Nuclear Elements (SINEs, 0.12% and 0.05%) and LTRs (21.67% and 15.57%) represented a larger part of the 14 chromosome sequences than of unanchored regions. The biggest difference in favor of unanchored regions was observed for unclassified retrotransposons which represents 16.76% of unanchored sequences against 3.28% of the 14 chromosome sequences. Main genome annotation statistics are synthesized in Table 1.

***V. planifolia* pangenomics and whole genome duplication**

The comparison of the four mosaic haplotypes from the two *V. planifolia* cultivars, CR0040 and Daphna (Supplemental Tables 12 and 13) showed that the 14 pseudomolecules of CR0040 were shorter and contained less genes than Daphna and that a large number of regions in the CR0040 pseudomolecules (haplotype A or B) were not located in the Daphna pseudomolecules

(Supplemental Figure 4). Pan-genomic analysis of the orthogroups from proteomes derived from the 14 chromosomes only (Supplemental Figure 5; Supplemental Table 14; Supplemental Note 4) indicated that the core genome was composed of 14,210 families and 77,692 genes (35,972 CR0040 and 41,720 Daphna). The dispensable genome of CR0040 contains 1,266 families and 3,613 genes specific to CR0040. The dispensable genome of Daphna contains 3,997 Daphna specific families and 13,645 genes. Finally, we looked at the expansion or reduction of gene families in relation to six proteomes (CR0040, Daphna, *Phalaenopsis equestris*, *Phalaenopsis aphrodite*, *A. thaliana*, *Oryza sativa*; Supplemental Figure 6). From an orchid perspective, the expansion number for the orchid node is rather low (+36) while the Daphna specific number is rather high (A +1841 and B +1943) compared to CR0040 (A +418 and B +826).

To identify whole genome duplications (WGD), pairwise genome synteny analyses between CR0040, Daphna, and *P. aphrodite,* and between themselves were carried out (Supplemental Figures 7 and 8, and Supplemental Notes 4 and 6). The CR0040 haplotype A dotplot validated at least one pan-orchid WGD (α°, the origin of the paleo-allotetraploid) previously found by Hasing et al. (2020). An additional dotplot diagonals and dS peak suggested a second WGD, possibly the tau of Monocots (τ^m).

Detection of non-endoreplicated regions

PE induce highly unbalanced DNA representation with a P/F DNA ratio ranging from 3 to 10 according to tissues. This was reflected in our assembly by highly variable sequencing depth (Figure 4A, green lane). The two random mosaic chromosomes which showed a low sequencing depth at most loci, may therefore contain a large part of the non-endoreplicated F fraction of the genome. It is likely that a large part of unanchored sequences originates from the two fully heterochromatinized chromosomes observed in the interphase nuclei (Figure 2I), possibly chromosome pairs 15 or 16). The remaining part of unanchored sequences should correspond to missing fractions in the anchored chromosomes. Interestingly, the sequencing reads mapping on CR0040 and Daphna assemblies also showed intra-chromosomal sequencing depth variations (Figure 4B). These patterns were consistent whatever the technology used. To observe this phenomenon globally on all chromosomes and genomes with all technologies (HiFi, ONT, Illumina), sequencing depth analysis tools were used and manual validation performed (Supplemental Note 5; Supplemental Tables 15 and 16). Two patterns of sequencing

depth variations have been identified along all chromosomes. The first one (indicated with a dotted box labeled "1" in Figure 4B and Supplemental Figure 9) corresponded to a sharp decrease of sequencing depth for both cultivars, with all sequencing technologies which dropped down from 45X-120X to less than 20X. Surprisingly, this pattern occurred independently on the two haplotypes. A total of 37 very low coverage regions (from 0.4 to 6 Mb in length) with this pattern were identified along the chromosomes (24 in haplotype A and 13 in haplotype B) for a cumulative size of 60.1 Mb. For a large part of these regions, we found low gene density and high repeat density. This pattern could correspond to non-endoreplicated regions present in both Daphna and CR0040 genomes. The fact that these patterns are systematically located on junctions between super-scaffolds is consistent with the decrease in sequencing depth inherent from non-endoreplication which impaired the assembly of the endoreplicated regions located on either side. The second pattern (indicated with a dotted box labeled "2" in Figure 4B and Supplemental Figure 9) corresponded to 36 regions (from 1.2 Mb to 20 Mb in length, cumulative size of 207.2 Mb) with segmental sequencing depth variation present in CR0040 (with HiFi, ONT and Illumina) but not in Daphna (with ONT and Illumina). Furthermore, these variations were syntenic along the two haplotypes but the direction of variation was inverted between the two phases. Their respective level of sequencing depth differs by a factor of about 3 in CR0040. The cause of these apparently coordinated sequencing depth inversions between CR0040 haplotypes remains unclear. After analyzing the locations of these k-mers in CR0040 assembly, it appeared that these low depth k-mers (between 5X and 15X) were mostly present in the unanchored part of the genome comparatively to the chromosome sequences (Figure 5) with median ratios values equal to 0.27 and 0.036 respectively, showing significant difference (Wilcoxon-Mann-Whitney test; p-value = 4e-13). However, chromosomes 7A and 6B were outliers, showing also a high proportion of low depth k-mers. In addition, the distribution of these k-mers along the genome was globally consistent with the areas identified except for some discrepancy (Supplemental Figure 10). Chromosomes 6B and 7A showed strong signals in terms of low depth k-mers proportions as already pointed out by Figure 5. Indeed, on chromosome 6B, k-mers of this type were positioned on nearly all the assembled sequence while they were localized on approximately half of the chromosome assembled 7A sequence.

Cell cycle regulator genes orthologs involved in *A. thaliana* endoreplication

The search for orthologs of the Cyclin-dependent Kinases (CDK) and cyclins (Cyc) families of *A. thaliana*, involved in regular endoreplication mechanism, showed that representatives of these two families were indeed found in the proteomes of CR0040 and *P. aphrodite* (Supplemental Table 17). However, the number of genes coding for CDKs and cyclins found via the orthogroups approach were lower for these two species. For example, the gene coding for Cyc-D3-1 in *A. thaliana* (At4g34160) was part of a species-specific orthogroup containing some other D-types cyclins genes. Regarding the genes encoding the regulatory proteins of the CDK/Cyc complexes, all of them had orthologs in both orchids. However, it appeared that these multigenic families were slightly underrepresented in CR0040 gene annotation compared to *A. thaliana* and *P. aphrodite*. Finally, an imbalance between the A and B haplotypes was observed for Fizzy-related proteins (Fzr) and cyclin-dependent kinase inhibitor (Krp) orthologs.

Vanilla genome hub

To support post-genomics efforts, the Vanilla Genome Hub (VGH, https://vanilla-genome-hub.cirad.fr) has been developed. It centralizes vanilla genomic information with a set of user-friendly interconnected modules and interfaces for analyzing and visualizing genomic data. From the main menu of VGH (Supplemental Note 6 and Figure 6A), the search for genes of interest to biologists is simplified using the interoperable system by the identification of paralogous genes by keywords and sequence homology (Figures 6B and 6C) and information report with gene name, gene localization and polypeptide function (Figure 6D). The genome browser was built to offer tracks of supplemental information such as: GC content, gene structure, gene expression, DNA sequencing depth and composition in repeats to support the identification of new genes of interest (Figure 6E, Supplemental Figure 11). A metabolic pathways reconstruction and visualization tool allows to identify the annotated genes involved in pathways (Figure 6F). A GO enrichment tool allows to test and visualize the enrichment according to a GO category of a gene group (Figure 6G). At last, comparative analysis at genome-scale is supported by an interactive multiscale synteny visualization (Figure 6H).

DISCUSSION

Flow cytometry and cytogenetic data validate the genome size and chromosome content

Genome size, ploidy level and chromosome content of the *V. planifolia* CR0040 cultivar were validated by FCM and cytogenetic analyses. The estimated size at 4.09 Gb indicated a ploidy level similar to other traditional diploid *V. planifolia* cultivars (Bory *et al.*, 2008; Lepers-Andrzejewski et al., 2011). Estimation of endoreplication levels confirmed PE as previously described in *V. planifolia* (Brown *et al.*, 2017). This species was shown to harbor diploidized meiotic chromosome pairing with 16 bivalents (Bory, 2007). This demonstrates the complete diploidization of this supposed segmental paleo-allotetraploid (Nair and Ravindran, 1994; Ravindran, 1979). The same meiotic observation has been also performed for *V.* × *tahitensis* by Lepers-Andrzejewski et al. (2011). Aneuploid chromosome numbers were frequently observed in mitotic metaphases of *V. planifolia* (Bory *et al.*, 2008; Nair and Ravindran, 1994), possibly due to the observed mitotic associations which could lead to unequal anaphase separation. This may lead to errors in the evaluation of the basic chromosome number, as it is the case in a recent paper where the authors considered that the basic number was x=14 (Hasing *et al.*, 2020). The phenomenon of aneuploidy apparently occurs only in somatic cells while meiosis appears to be regular with a stable number of chromosomes (Bory, 2007). Although the CR0040 assembly is more complete than that of Daphna, only 14 pseudomolecules were obtained because CR0040 scaffolds were anchored on the 14 Daphna pseudomolecules. Chromosomes 15 and 16 are probably not endoreplicated and present in the unanchored part (CR0040_A0 and CR0040_B0).

PE hinders whole genome assembly

Given the CR0040 diploid genome size estimated to 4.09 Gb using FCM, our genome assembly represented around 83% of the expected genome size which was twice the size of the Daphna genome previously published (Hasing *et al.*, 2020). This difference could be explained by the fact that the assembly for CR0040 was done from HiFi reads which allowed to assemble in different contigs the repeated regions despite their low sequencing depth. We were thus able to assemble a greater number of repeated sequences that might correspond to a large fraction of the non-endoreplicated genome, missing from the Daphna genome assembly. The biological reality of this hypothesis is reinforced by the consistency of k-mer depth profiles and sequencing depth patterns resulting from the mapping of reads from different sequencing

technologies (HiFi, 10X and ONT) tested in this study for CR0040 (Supplemental Figure 9). A k-mer spectra-cn diagram is an efficient tool to visually compare reads and assembly k-mer compositions. They are used to validate diploid or haploid assembly quality (Yen et al., 2020). The k-mer spectra-cn diagram shows clearly a diploid general pattern with a heterozygous distribution containing only k-mers in single copy in the assembly and a homozygous distribution harboring, as expected, only k-mers present twice in the assembly. Unexpectedly for a diploid genome, this figure includes a third distribution which is located in the low coverage area of the diagram. The color pattern shows clearly that these k-mers present in low frequencies (5 to 15 times) are also present in our assembly. These k-mers represent the non-repeated fraction of low coverage sections of the assembly which are mainly located in the unanchored sequences but are also present in low coverage sections of the other chromosomes. Even if the unanchored sequences are mainly built of repeats they also harbor genes and other non-repeated blocks and these parts are large enough in terms of k-mers to generate this unexpected k-mer distribution in the spectra-cn plot. These k-mers are not present in the public *V. planifolia* Daphna assembly and therefore the corresponding distribution is black in Figure 3B.

Molecular signatures of partial endoreplication

The abundance of interspersed repeats detected in CR0040 was consistent with already mentioned data in other orchids such as *Phalaenopsis equestris* (Cai et al., 2015) and *P. aphrodite* (Chao et al., 2018) and in other lineages, like the *Oryza* genus (Stein et al., 2018). High content of retrotransposons and low content in DNA transposons were in the range of what has been found for different orchids (Cai et al., 2015; Chao et al., 2018). High repeat content was found in candidate non-endoreplicated regions, which is in agreement with what has already been described in other orchids (Chumová et al., 2021). Furthermore, some types of repeats might be preferentially found in non-endoreplicated regions as shown by repeats proportions differences between assembled chromosomes and unanchored sequences, and in particular retrotransposons proportions. Thus, LINEs for example, occupy a larger portion of the unanchored regions than that of the 14 chromosomes even though these regions are overrepresented in the present assembly. However, the lack of a more detailed annotation of the retrotransposons class hampers the search for a potential preferential distribution of repeat families between endoreplicated and non-endoreplicated regions. It is therefore crucial to better

annotate these repeats in order to determine exactly which kinds are preferentially found in the two fractions of the genome. On the other hand, the distribution of genes in the genome shows the opposite trend with approximately two-third of the protein coding sequences localized in the anchored region.

The distinct sequencing depth profiles observed between CR0040 and Daphna likely reflected a tissue-specific endoreplication pattern. Indeed, the nodes used for sequencing CR0040 genome are growing and differentiating tissues while the leaves used for sequencing Daphna genome are made of fully differentiated cells. The irregular haplotype-specific endoreplication pattern (segmental or not) observed in CR0040 could thus result from a peculiar physiological activity. Whatever the reason, this intriguing pattern suggests a complex and fine regulation of PE at chromosome level which deserves further studies. While no previous study has demonstrated the mechanisms underlying PE in orchids, many works have focused on the regulation of regular endoreplication found in a large number of plant species, and well analyzed on tomato and Arabidopsis (Lang and Schnittger, 2020). The common mechanism to trigger endoreplication is a downregulation of mitotic CDK activity to suppress the mitosis and a fine regulation of this activity throughout the induced endocycle with an alternance between high and low activity levels at specific checkpoints in order to maintain the replication process (De Veylder et al., 2011; Shimotohno et al., 2021). CDK controls cell cycle progression and mitosis entry via its phosphorylation activity, which is activated by association with CYC proteins. Recently, Inada et al. (2021) demonstrated the involvement of actin and actin-binding protein in the regulation of *A. thaliana* endoreplication. The whole genome analysis made it possible to identify orthologous CDK, cyclins, CDK-activators/repressors and Actin Depolymerizing Factors (ADF) in *V. planifolia* CR0040. A first step in understanding orchid PE would therefore be to further analyze these molecular regulators. Indeed, the recognition of orthologs and paralogs in large gene families, such as CDK-cyclin complex, is challenging and requires deepening by a high-quality manual annotation of the genes of interest (Vaattovaara et al., 2019).

Even though PE seems specific to orchids in plants (Trávníček et al., 2015), such phenomenon of under-represented genomic regions is well known in metazoan. Ciliates such as *Paramecium tetraurelia* or *Tetrahymena thermophile* show programmed DNA elimination following endoreplication in their MAC nucleus, involving chromosome fragmentation and elimination of specific sequences called IES (Internal Eliminated Sequences) (Sellis, 2021; Bracht et al., 2013). However, FCM approaches on *Ludisia discolor*, an orchid subject to PE, have ruled out

the hypothesis of such DNA elimination and favor that of under-replication (Hřibová et al., 2016). Under-replication has also been studied in several organisms such as Drosophila for which it has been proposed that a reduction in expression of genes involved in DNA replication may lead to a slower mitosis S-phase, and an incomplete replication of genomic regions during late S-phase (Lilly and Spradling, 1996). Molecular mechanisms described in Drosophila highlighted an inhibition of the replication fork progression involving Rif1 protein, which interacts with the SUUR protein (Munden et al., 2018; Armstrong et al., 2019).

Finally, cytogenetic studies using *in situ* hybridization techniques (FISH, fluorescence *in situ* hybridization, and GISH, genomic *in situ* hybridization) could also be used to increase our knowledge of the molecular signatures of PE (Younis et al., 2015). Recent advance in FISH is the development of probes based on synthetic oligonucleotides specific to repetitive sequences or to particular chromosome regions (Jiang, 2019). This new-generation of FISH probes in plants was applied to species with a sequenced genome, for example for *Zea* and *Cucumis* species (Braz et al., 2020; Han et al., 2015; Martins et al., 2019; Zhang et al., 2021a). Endoreplicated versus non-endoreplicated genomic regions could serve to synthesize oligo-based FISH probes specific to each fraction for precisely locating these PE signatures on chromosomes. GISH technique uses the total genomic DNA of a species, in contrast to FISH. We hypothesize that hybridizing the total DNA of highly endoreplicated nuclei (16E, 32E) to CR0040 chromosomes would induce a more intense hybridization signal in endoreplicated regions, which would allow us to identify non-endoreplicated areas with little hybridization.

Impact of technologies on whole genome evolution analysis

The strategy of combining optical mapping and HiFi long reads sequencing for CR0040 genome assembly resulted in a haplotype A with 14 pseudomolecules of better quality and with less scaffolding errors than Daphna haplotype A, which was built with Hi-C and ONT technologies (Hasing et al., 2020). Indeed, comparisons between Daphna and CR0040 haplotypes A revealed a dual haplotype conservation problem in the Daphna phased assembly, which is reflected in the Daphna Hi-C scaffolding. The use of HiFi long-reads and optical maps allowed for more accurate haplotype separation as shown in previous works (Du et al., 2020; Matthews et al., 2018). In the case of CR0040 not only did HiFi allow better assembly of non-endoreplicated regions, but HiFiasm allowed better separation of haplotypes. These

improvements were therefore necessary to better solve the sequencing of the complex vanilla genome, with a high rate of heterozygosity (Ho *V. planifolia* cultivars = 0.362; Favre et al., 2022) and subjected to PE (Brown *et al.*, 2017). However, this dual haplotype conservation problem observed in Daphna, and not in CR0040, impacted comparative pan-genomics analyses and distorted results obtained. Thus, the differences observed between the two genomes of *V. planifolia* (number of paralogs, numbers of gene families with expansions/contractions, complete and duplicated BUSCO scores) could be explained by these mosaic assembly problems and therefore an incorrect separation between haplotypes A and B. Monocot genome evolution analyzes were carried out using the high-quality haplotype A sequence of CR0040. Dotplot results were in agreement with the fact that *V. planifolia* is a diploidized paleo-polyploid species with primary basic chromosome number *x*=8 and secondary basic number *x*=16, as described for the whole *Vanilla* genus (Felix and Guerra, 2005). Moreover, only one locus (two spots) of rDNA (18S-5.8S-26S) was identified in the genome of *V. planifolia* by cytogenetic approaches, which brings one additional evidence of an ancient diploidization of this supposed segmental paleo-allotetraploid. Finally, two WGDs, possibly corresponding to α° and τ^{m}, were highlighted, as also described for the *Dendrobium chrysotoxum* chromosome-scale genome assembly (Zhang et al., 2021b).

Efficiency of the integrative approach combining cytogenetics and high-quality whole genome sequencing

In this study, we confirmed the size and structure of the *V. planifolia* genome using both cytogenetics and nuclear DNA sequencing methods. The particular phenomenon of PE at play in many orchids has been explored at chromosome level, for the first time in plants to our knowledge. Our data showed that the non-endoreplicated sequences are very predominantly made up of repeated sequences. This confirmed, at the genomic level, previous findings in orchids by Chumová et al. (2021), based on Phylogenetics Generalised Least Squares (PGLS) model, and by Brown et al. (2017) who demonstrated in *Vanilla* by nuclei imaging that, on the other hand, the endoreplicated part was transcribed. We nevertheless revealed that 33% of the 59,128 protein coding genes annotated were present in the two random mosaic chromosomes corresponding mainly to the non-endoreplicated part as shown by low-sequencing depth. In addition, a thorough examination of the sequencing depths along anchored chromosomes with three different technologies has revealed 73 regions that appear with different endoreplication

levels that vary with haploid phase. Half of which may be linked to tissue type (leaves *vs* nodes). This last conclusion has to be confirmed with DNA sequencing from different tissues of the same cultivar. This work constitutes a considerable progress in the knowledge of *V. planifolia* genomics and sheds light on the most relevant methodologies for further deciphering this complex genome and the PE phenomenon. The Vanilla Genome Hub was built to help the community to address major unresolved questions about vanilla such as PE, biosynthesis of aromatic compounds, and resistance to pathogens. We are working on a new version of the vanilla nuclear genome sequence that will be improved in terms of haplotype separation, chromosome reconstruction, gene and repeat element annotation in order to further investigate the molecular mechanisms of PE with appropriate plant material, bio-technologies and bioinformatics tools.

MATERIALS AND METHODS

Cytometry, cytogenetics and DNA sequencing

A traditional vanilla cultivar (CR0040) from Reunion island was used in this study (Supplemental Note 1). FCM and cytogenetics studies were performed using protocols described in (Supplemental Note 1). High molecular weight (HMW) DNA and ultra-HMW DNA was extracted from node tissues and sequenced using PacBio HiFi, ONT and Illumina technologies (Supplemental Note 1). Optical genome maps were produced using Bionano Genomics® protocol and the Saphyr G1 System (Supplemental Note 1).

Genome assembly and analysis

HiFi reads were assembled into contigs using hifiasm 0.13 with default parameters (Cheng et al., 2021). The hybrid scaffolding was performed between DNA contigs and optical genome maps using the hybrid Scaffold pipeline of Bionano Genomics® with default parameters. These scaffolds were phased into two haplotypes using in house scripts and the not-scaffolded contigs were phased using purge dups (https://github.com/dfguan/purge_dups). Then, pseudomolecules were reconstructed using alignments of the phased-assembly on Daphna chromosomes (Hasing et al., 2020, Supplemental Note 2). The assembly quality was estimated

with quast 5.1.0 (Gurevich et al., 2013) and using the approach of Benchmarking Universal Single-Copy Orthologs (BUSCO, version 5.0.0) (Simao et al., 2015) (Supplemental Note 2). The k-mers analysis was performed with kat 2.4.2 using the comp tool (Mapleson et al., 2017). The plot script was slightly modified to project on the Y axis the number of distinct k-mers multiplied by the k-mers multiplicity instead of just the number of distinct k-mers. In parallel, the k-mers of size 47 having a depth between 5 and 15 were extracted within PacBio sequences using Jellyfish 2.3.0 (Marcais and Kingsford, 2011). These k-mers were repositioned on our reference using the tool 'query_per_sequence' (https://github.com/gmarcais/Jellyfish/tree/master/examples/query_per_sequence) and the ratio of these k-mers was computed among each sequence of our genome. These sequences were splitted between chromosomes and unanchored sequences and the repartition of the k-mer ratio was drawn using python seaborn library (https://seaborn.pydata.org/).

Structural and functional genome annotation

Automatic gene prediction was performed on CR0040 contigs with the EuGene Eukaryotic Pipeline (EGNEP version 1.5) (Sallet et al., 2019) (Supplemental Note 3). Transcriptomic data from CR0040 were produced using RNA sequencing of nine organs with Illumina technology (Supplemental Note 3). In addition, gene expression profiles and putative novel isoforms were identified with Stringtie v. 2.0.3 (Kim et al., 2019) (Supplemental Note 3). Transcriptomic data from *V. planifolia* cultivars (CR0040, Daphna (ncbi Bioprojects: PRJNA668740 and PRJNA633886), and an unspecified cultivar (ncbi GEO: GSE134155)), proteomic data from *V. planifolia* Daphna (Hasing et al., 2020), *Phalaenopsis equestris* (ncbi Bioproject: PRJNA382149) and the *Liliopsida* class (Swissprot 2020_06), as well as a custom orchids specific statistical model for splice site detection were used for this analysis (Supplemental Note 3). Functions were assigned through InterProScan domain searches as well as similarity searches against Uniprot/Swissprot and Uniprot/TrEMBL databases (BlastP). Gene Ontology (GO) terms were assigned through InterProScan (Jones et al., 2014) results while Enzyme Classification (EC) numbers were predicted combining both tools PRIAM (Claudel-Renard et al., 2003) and BlastKOALA (Kanehisa et al., 2016).

Repeats were first identified using RepeatModeler v2.0.1 (Flynn et al., 2020), RepeatScout v1.0.5 and transposable element genes predicted from EGNEP annotation and then classified with REPET v3.0 (Flutre et al., 2011) and PASTEC v2.0 (Hoede et al., 2014) according to the

Wicker's TE classification (Wicker et al., 2007). After cleaning steps (see details in note S9.2), repeats were clustered with CD-HIT v4.8.1 (Fu et al., 2012) to produce two banks of repeats. The CR0040 genome was then annotated for repeats using previous banks, RepeatMasker v4.1.1 (Tarailo-Graovac and Chen, 2009) and bedtools intersect v2.29.2 (Quinlan and Hall, 2010).

Genomic comparisons and gene family's reconstruction

In order to compare the 14 haplotype A chromosomes of both vanilla cultivars, to check the completeness of the Vanilla genome and to study the pan-orchid α° WGD, a series of analyses were performed with the CoGe Synmap pipeline as described in Supplemental Note 4. Gene family reconstruction was performed using Orthofinder2 (v.2.4.0) (Emms and Kelly, 2019). Genes known to be involved in cell cycle control in *A. thaliana* such as Cyclins (Cyc), Cyclin-Dependent Kinases (CDKs) and known regulators of these genes were searched in CR0040 and *P. aphrodite* proteomes with a combination of Blastp searches and orthogroups. This analysis was applied on CDK-A and -B types as well as Cyc-A -B -D types. Regulators of these genes included cyclin-dependent kinase inhibitor (KRP), transcriptional repressor ILP1, WEE1, Actin-Depolymerizing Factor (ADF), Fizzy-Related proteins (FZR).

Detection of non-endoreplicated genomic regions

Reads from each sequencing technology used in this study (HiFi, ONT and Illumina reads from CR0040), as well as ONT and Illumina reads from Daphna were mapped on the CR0040 assembly. Illumina short-reads and long-reads (HiFi and ONT) were mapped on CR0040 assembly using bwa-mem2 (Vasimuddin et al., 2019) and Minimap2 (Li, 2018), respectively. Sequencing depths were averaged for genomic windows of 20 kb. To detect sequencing depth bias and to limit the risk to detect false positives, the mean of sequencing depth for every 20 successive windows of 20 kb was computed using Illumina reads for Daphna and using long-reads (HiFi and ONT) for CR0040. Identified regions were manually validated and refined by visualization of sequencing depth drops for each CR0040 chromosome and for all available sequencing datasets (see details in Supplemental Note 5).

Vanilla Genome Hub (VGH)

The VGH was constructed using the Tripal system, a specific toolkit for the construction of online community genomic databases, by integrating the GMOD Chado database schema and the Drupal open source platform (https://www.drupal.org/). The VGH implements a set of interconnected modules and user-friendly interfaces (details in Supplemental Note 6).

Data availability

The chromosome assembly and accompanying data received the following identifiers in NCBI: BioProject (with SRA database) ID PRJNA753216, (haplotype A) and PRJNA754028 (haplotype B) BioSample (node) SAMN20691751. Data can be accessed at the vanilla genome hub site (see below).

RNA-Seq data are readily accessible on the NCBI portal : BioSamples SAMN20691786 (fruit), SAMN20691787 (leaf), SAMN20691788 (flower), SAMN20691789 (stem), SAMN20691790 (soil root), SAMN20691791 (aerial root), SAMN20691792 (bud), SAMN20691793 (flower bud), SAMN20691794 (ovary), SAMN20691795 (mixed tissues); SRA : SRR15411867 (mixed tissues), SRR15411868 (ovary), SRR15411869 (flower bud), SRR15411870 (bud), SRR15411871 (aerial root), SRR15411872 (soil root), SRR15411873 (stem), SRR15411874 (flower), SRR15411875 (leaf), SRR15411876 (fruit)

In addition, these data and various exploration tools are accessible at “Vanilla Genome Hub” (https://vanilla-genome-hub.cirad.fr/).

AUTHORS CONTRIBUTIONS

C.J., M.D., M.G., P.B. contributed to conceptualization of the study.

C.C., C.J., G.S., M.B., M.D., O.B., S.B., W.M. designed the experiments.

M.B., S.S-Y. performed flow cytometry and cytogenetic experiments and analyses.

L.B., J.Z. contributed to the funding of the research, monitored the progress of the work and supported the researchers throughout the project

C.C., C.L.R., O.B., W.M. performed nucleic acid preparation and sequencing.

C.C., C.J., C.K., G.D., G.S., Q.P., S.B., W.M. performed sequences analyses and assemblies.

C.C., G.D., Q.P., S.B., S.L.A performed genome annotation and built the genome hub

C.C., C.J., C.K, M.G., Q.P. and W.M. outlined the manuscript and wrote first drafts.

C.C., C.J., C.K., C.L.R., G.D., G.S., M.B., M.D., M.G., P.B., Q.P., S.B., S.S-Y., W.M. contributed with inputs and revisions in the manuscripts.

The authors declare that they have no conflict of interests.

ACKNOWLEDGMENTS

We are grateful to Jean Bernard Dijoux and Katia Jade for preparing the plant material, and to the Plant Protection Platform (3P, IBISA) for lab facilities and plant resources access (BRC Vatel). We acknowledge the SouthGreen Bioinformatics Platform (http://www.southgreen.fr/) for computational resources access and the GeT-PlaGe platform (INRAE, Toulouse, France) for the use of sequencing facilities. Finally, the authors would like to thank the reviewers for their suggestions which helped to improve the manuscript.

FUNDING

This work was supported by grants from Eurovanille and V. Mane Fils companies. The research was co-funded by the Centre de Coopération Internationale en Recherche Agronomique pour le Développement (CIRAD), the Université de la Réunion (UR), the Institut National de Recherche pour l'Agriculture l'Alimentation et l'Environnement (INRAE), the Centre National de la Recherche Scientifique (CNRS), and the Etablissement Vanille de Tahiti (EVT). This work was also granted by the European Regional Development Fund (ERDF), the Conseil Régional de la Réunion, and the Conseil Départemental de la Réunion.

REFERENCES

Armstrong, R. L., Penke, T., Chao, S. K., Gentile, G. M., Strahl, B. D., Matera, A. G., McKay, D. J., & Duronio, R. J. (2019). H3K9 Promotes Under-Replication of Pericentromeric Heterochromatin in Drosophila Salivary Gland Polytene Chromosomes. Genes, 10(2), 93. 10.3390/genes10020093

Bhosale, R., Boudolf, V., Cuevas, F., Lu, R., Eekhout, T., Hu, Z.B., Van Isterdael, G., Lambert, G.M., Xu, F., Nowack, M.K., et al. (2018). A Spatiotemporal DNA Endoploidy Map of the Arabidopsis Root Reveals Roles for the Endocycle in Root Development and Stress Adaptation. Plant Cell **30**:2330-2351. 10.1105/tpc.17.00983.

Bory, S. (2007). Diversity of *Vanilla planifolia* in the Indian ocean and its related species : Genetics, cytogenetics and epigenetics aspect. Université de La Réunion, France.

Bory, S., Catrice, O., Brown, S., Leitch, I.J., Gigant, R., Chiroleu, F., Grisoni, M., Duval, M.F., and Besse, P. (2008). Natural polyploidy in *Vanilla planifolia* (Orchidaceae). Genome **51**:816-826. 10.1139/G08-068.

Bourdon, M., Pirrello, J., Cheniclet, C., Coriton, O., Bourge, M., Brown, S., Moise, A., Peypelut, M., Rouyere, V., Renaudin, J.P., et al. (2012). Evidence for karyoplasmic homeostasis during endoreduplication and a ploidy-dependent increase in gene transcription during tomato fruit growth. Development **139**:3817-3826. 10.1242/dev.084053.

Bracht, J. R., Fang, W., Goldman, A. D., Dolzhenko, E., Stein, E. M., & Landweber, L. F. (2013). Genomes on the edge: programmed genome instability in ciliates. Cell, 152(3), 406–416. https://doi.org/10.1016/j.cell.2013.01.005

Braz, G.T., Martins, L.D., Zhang, T., Albert, P.S., Birchler, J.A., and Jiang, J.M. (2020). A universal chromosome identification system for maize and wild Zea species. Chromosome Research **28**:183-194. 10.1007/s10577-020-09630-5.

Brown, S.C., Bourge, M., Maunoury, N., Wong, M., Bianchi, M.W., Lepers-Andrzejewski, S., Besse, P., Siljak-Yakovlev, S., Dron, M., and Satiat-Jeunematre, B. (2017). DNA Remodeling by Strict Partial Endoreplication in Orchids, an Original Process in the Plant Kingdom. Genome Biology and Evolution **9**:1051-1071. 10.1093/gbe/evx063.

Cai, J., Liu, X., Vanneste, K., Proost, S., Tsai, W.C., Liu, K.W., Chen, L.J., He, Y., Xu, Q., Bian, C., et al. (2015). The genome sequence of the orchid *Phalaenopsis equestris*. Nat Genet **47**:65-72. 10.1038/ng.3149.

Chao, Y.T., Chen, W.C., Chen, C.Y., Ho, H.Y., Yeh, C.H., Kuo, Y.T., Su, C.L., Yen, S.H., Hsueh, H.Y., Yeh, J.H., et al. (2018). Chromosome-level assembly, genetic and physical mapping of *Phalaenopsis aphrodite* genome provides new insights into species adaptation and resources for orchid breeding. Plant Biotechnol J **16**:2027-2041. 10.1111/pbi.12936.

Cheng, H., Concepcion, G.T., Feng, X., Zhang, H., and Li, H. (2021). Haplotype-resolved de novo assembly using phased assembly graphs with hifiasm. Nat Methods **18**:170-175. 10.1038/s41592-020-01056-5.

Chumová, Z., Záveská, E., Hloušková, P., Ponert, J., Schmidt, P. A., Čertner, M., Mandáková, T., & Trávníček, P. (2021). Repeat proliferation and partial endoreplication jointly shape the patterns of genome size evolution in orchids. The Plant Journal : for cell and molecular biology, **107(2)**:511–524. 10.1111/tpj.15306

Claudel-Renard, C., Chevalet, C., Faraut, T., and Kahn, D. (2003). Enzyme-specific profiles for genome annotation: PRIAM. Nucleic acids research, 31(22), 6633–6639. 10.1093/nar/gkg847

De Veylder, L., Larkin, J.C., and Schnittger, A. (2011). Molecular control and function of endoreplication in development and physiology. Trends in Plant Science **16**:624-634. 10.1016/j.tplants.2011.07.001.

Doležel J, Bartoš J, Voglmayr H, Greilhuber J. (2003). Nuclear DNA content and genome size of trout and human. Cytom. Part A. **51**A:127–128. doi: 10.1002/cyto.a.10013.

Du, K., Stock, M., Kneitz, S., Klopp, C., Woltering, J.M., Adolfi, M.C., Feron, R., Prokopov, D., Makunin, A., Kichigin, I., et al. (2020). The sterlet sturgeon genome sequence and the mechanisms of segmental rediploidization. Nat Ecol Evol **4**:841-852. 10.1038/s41559-020-1166-x.

Emms, D.M., and Kelly, S. (2019). OrthoFinder: phylogenetic orthology inference for comparative genomics. Genome Biology **20**Artn 238. 10.1186/S13059-019-1832-Y.

Favre, F., Jourda, C., Grisoni, M., Piet, Q., Rivallan, R., Dijoux, J.B., Hascoat, J., Lepers-Andrzejewski, S., Besse, P., and Charron, C. (2022). A genome-wide assessment of the genetic diversity, evolution and relationships with allied species of the clonally propagated crop *Vanilla planifolia* Jacks. ex Andrews. Genet Resour Crop Ev. 10.1007/s10722-022-01362-1.

Felix, L.P., and Guerra, M. (2005). Basic chromosome numbers of terrestrial orchids. Plant Syst Evol **254**:131-148. 10.1007/s00606-004-0200-9.

Flutre, T., Duprat, E., Feuillet, C., and Quesneville, H. (2011). Considering Transposable Element Diversification in De Novo Annotation Approaches. Plos One **6**ARTN e16526 10.1371/journal.pone.0016526.

Flynn, J.M., Hubley, R., Goubert, C., Rosen, J., Clark, A.G., Feschotte, C., and Smit, A.F. (2020). RepeatModeler2 for automated genomic discovery of transposable element families. Proceedings of the National Academy of Sciences of the United States of America **117**:9451-9457. 10.1073/pnas.1921046117.

Fu, L.M., Niu, B.F., Zhu, Z.W., Wu, S.T., and Li, W.Z. (2012). CD-HIT: accelerated for clustering the next-generation sequencing data. Bioinformatics **28**:3150-3152. 10.1093/bioinformatics/bts565.

Gurevich, A., Saveliev, V., Vyahhi, N., and Tesler, G. (2013). QUAST: quality assessment tool for genome assemblies. Bioinformatics **29**:1072-1075. 10.1093/bioinformatics/btt086.

Han, Y.H., Zhang, T., Thammapichai, P., Weng, Y.Q., and Jiang, J.M. (2015). Chromosome-Specific Painting in Cucumis Species Using Bulked Oligonucleotides. Genetics **200**:771-779. 10.1534/genetics.115.177642.

Hasing, T., Tang, H.B., Brym, M., Khazi, F., Huang, T.F., and Chambers, A.H. (2020). A phased *Vanilla planifolia* genome enables genetic improvement of flavour and production. Nat Food **1**:811-819. 10.1038/s43016-020-00197-2.

Hoede, C., Arnoux, S., Moisset, M., Chaumier, T., Inizan, O., Jamilloux, V., and Quesneville, H. (2014). PASTEC: An Automatic Transposable Element Classification Tool. Plos One **9**ARTN e91929.10.1371/journal.pone.0091929.

Hřibová, E., Holušová, K., Trávníček, P., Petrovská, B., Ponert, J., Šimková, H., Kubátová, B., Jersáková, J., Čurn, V., Suda, J., Doležel, J., & Vrána, J. (2016). The Enigma of Progressively Partial Endoreplication: New Insights Provided by Flow Cytometry and Next-Generation Sequencing. Genome biology and evolution, **8(6)**:1996–2005. https://doi.org/10.1093/gbe/evw141.

Inada, N., Takahashi, N., and Umeda, M. (2021). Arabidopsis thaliana subclass I ACTIN DEPOLYMERIZING FACTORs and vegetative ACTIN2/8 are novel regulators of endoreplication. Journal of Plant Research **134**:1291-1300. 10.1007/s10265-021-01333-0.

Jiang, J.M. (2019). Fluorescence *in situ* hybridization in plants: recent developments and future applications. Chromosome Research **27**:153-165. 10.1007/s10577-019-09607-z.

Jones, P., Binns, D., Chang, H. Y., Fraser, M., Li, W., McAnulla, C., McWilliam, H., Maslen, J., Mitchell, A., Nuka, G., Pesseat, S., Quinn, A. F., Sangrador-Vegas, A., Scheremetjew, M., Yong, S. Y., Lopez, R., & Hunter, S. (2014). InterProScan 5: genome-scale protein function classification. Bioinformatics (Oxford, England), 30(9), 1236–1240. 10.1093/bioinformatics/btu031

Kanehisa, M., Sato, Y., & Morishima, K. (2016). BlastKOALA and GhostKOALA: KEGG Tools for Functional Characterization of Genome and Metagenome Sequences. Journal of molecular biology, *428*(4), 726–731. https://doi.org/10.1016/j.jmb.2015.11.006

Kim, D., Paggi, J.M., Park, C., Bennett, C., and Salzberg, S.L. (2019). Graph-based genome alignment and genotyping with HISAT2 and HISAT-genotype. Nature Biotechnology **37**:907-+. 10.1038/s41587-019-0201-4.

Lang, L., and Schnittger, A. (2020). Endoreplication - a means to an end in cell growth and stress response. Current Opinion in Plant Biology **54**:85-92. 10.1016/j.pbi.2020.02.006.

Lee, H.O., Davidson, J.M., and Duronio, R.J. (2009). Endoreplication: polyploidy with purpose. Genes Dev **23**:2461-2477. 10.1101/gad.1829209.

Lepers-Andrzejewski, S., Siljak-Yakovlev, S., Brown, S.C., Wong, M., and Dron, M. (2011). Diversity and Dynamics of Plant Genome Size: An Example of Polysomaty from a Cytogenetic Study of Tahitian Vanilla (Vanilla X Tahitensis, Orchidaceae). American Journal of Botany **98**:986-997. 10.3732/ajb.1000415.

Li, H. (2018). Minimap2: pairwise alignment for nucleotide sequences. Bioinformatics **34**:3094-3100.

Lilly, M. A., & Spradling, A. C. (1996). The Drosophila endocycle is controlled by Cyclin E and lacks a checkpoint ensuring S-phase completion. Genes & development, 10(19), 2514–2526. 10.1101/gad.10.19.2514

Mapleson, D., Accinelli, G.G., Kettleborough, G., Wright, J., and Clavijo, B.J. (2017). KAT: a K-mer analysis toolkit to quality control NGS datasets and genome assemblies. Bioinformatics **33**:574-576. 10.1093/bioinformatics/btw663.

Marcais, G., and Kingsford, C. (2011). A fast, lock-free approach for efficient parallel counting of occurrences of k-mers. Bioinformatics **27**:764-770. 10.1093/bioinformatics/btr011.

Martins, L.D., Yu, F., Zhao, H.N., Dennison, T., Lauter, N., Wang, H.Y., Deng, Z.H., Thompson, A., Semrau, K., Rouillard, J.M., et al. (2019). Meiotic crossovers characterized by haplotype-specific chromosome painting in maize. Nature Communications **10**Artn 4604 10.1038/S41467-019-12646-Z.

Matthews, B.J., Dudchenko, O., Kingan, S.B., Koren, S., Antoshechkin, I., Crawford, J.E., Glassford, W.J., Herre, M., Redmond, S.N., Rose, N.H., et al. (2018). Improved reference genome of *Aedes aegypti* informs arbovirus vector control. Nature **563**:501-+. 10.1038/s41586-018-0692-z.

Munden, A., Rong, Z., Sun, A., Gangula, R., Mallal, S., & Nordman, J. T. (2018). Rif1 inhibits replication fork progression and controls DNA copy number in Drosophila. eLife, *7*, e39140. 10.7554/eLife.39140

Nair, R.R., and Ravindran, P.N. (1994). Somatic Association of Chromosomes and Other Mitotic Abnormalities in *Vanilla planifolia* (Andrews). Caryologia **47**:65-73. Doi 10.1080/00087114.1994.10797284.

Perez-Silva, A., Odoux, E., Brat, P., Ribeyre, F., Rodriguez-Jimenes, G., Robles-Olvera, V., Garcia-Alvarado, M.A., and Gunata, Z. (2006). GC-MS and GC-olfactometry analysis of aroma compounds in a representative organic aroma extract from cured vanilla (*Vanilla planifoli*a G. Jackson) beans. Food chemistry **99**:728-735. 10.1016/j.foodchem.2005.08.050.

Quinlan, A.R., and Hall, I.M. (2010). BEDTools: a flexible suite of utilities for comparing genomic features. Bioinformatics **26**:841-842.

Ravindran, P.N. (1979). Nuclear Behavior in the Sterile Pollen of *Vanilla planifolia* (Andrews). Cytologia **44**:391-396. DOI 10.1508/cytologia.44.391.

Sallet, E., Gouzy, J., and Schiex, T. (2019). EuGene: An Automated Integrative Gene Finder for Eukaryotes and Prokaryotes. Gene Prediction: Methods and Protocols **1962**:97-120. 10.1007/978-1-4939-9173-0_6.

S**ellis, D., Guérin, F., Arnaiz, O., Pett, W., Lerat, E., Boggetto, N., Krenek, S., Berendonk, T., Couloux, A., Aury, J. M., Labadie, K., Malinsky, S., Bhullar, S., Meyer, E., Sperling, L., Duret, L., & Duharcourt, S.** (2021). Massive colonization of protein-coding exons by selfish genetic elements in Paramecium germline genomes. PLoS biology, 19(7), e3001309. 10.1371/journal.pbio.3001309

Shimotohno, A., Aki, S.S., Takahashi, N., and Umeda, M. (2021). Regulation of the Plant Cell Cycle in Response to Hormones and the Environment. Annual Review of Plant Biology, Vol 72, 2021 **72**:273-296. 10.1146/annurev-arplant-080720-103739.

Simao, F.A., Waterhouse, R.M., Ioannidis, P., Kriventseva, E.V., and Zdobnov, E.M. (2015). BUSCO: assessing genome assembly and annotation completeness with single-copy orthologs. Bioinformatics **31**:3210-3212. 10.1093/bioinformatics/btv351.

Stein, J.C., Yu, Y., Copetti, D., Zwickl, D.J., Zhang, L., Zhang, C., Chougule, K., Gao, D., Iwata, A., Goicoechea, J.L., et al. (2018). Genomes of 13 domesticated and wild rice relatives highlight genetic conservation, turnover and innovation across the genus *Oryza*. Nat Genet **50**:285-296. 10.1038/s41588-018-0040-0.

Tarailo-Graovac, M., and Chen, N. (2009). Using RepeatMasker to identify repetitive elements in genomic sequences. . In Current protocols in bioinformatics A.D. Baxevanis, ed.

Trávníček, P., Čertner, M., Ponert, J., Chumová, Z., Jersáková, J., & Suda, J. (2019). Diversity in genome size and GC content shows adaptive potential in orchids and is closely

linked to partial endoreplication, plant life-history traits and climatic conditions. The New phytologist, **224(4)**:1642–1656. https://doi.org/10.1111/nph.15996.

Trávníček, P., Ponert, J., Urfus, T., Jersáková, J., Vrána, J., Hřibová, E., Doležel, J., & Suda, J. (2015). Challenges of flow-cytometric estimation of nuclear genome size in orchids, a plant group with both whole-genome and progressively partial endoreplication. Cytometry. Part A : the journal of the International Society for Analytical Cytology, **87(10)**:958–966. https://doi.org/10.1002/cyto.a.22681.

Vaattovaara, A., Leppälä, J., Salojärvi, J., & Wrzaczek, M. (2019). High-throughput sequencing data and the impact of plant gene annotation quality. Journal of experimental botany, **70(4)**:1069–1076. https://doi.org/10.1093/jxb/ery434.

Vasimuddin, M., Misra, S., Li, H., and Aluru, S. (2019). Efficient Architecture-Aware Acceleration of BWA-MEM for Multicore Systems. Int Parall Distrib P:314-324. 10.1109/Ipdps.2019.00041.

Wicker, T., Sabot, F., Hua-Van, A., Bennetzen, J.L., Capy, P., Chalhoub, B., Flavell, A., Leroy, P., Morgante, M., Panaud, O., et al. (2007). A unified classification system for eukaryotic transposable elements. Nat Rev Genet **8**:973-982. nrg2165 [pii] 10.1038/nrg2165.

Yen, E.C., McCarthy, S.A., Galarza, J.A., Generalovic, T.N., Pelan, S., Nguyen, P., Meier, J.I., Warren, I.A., Mappes, J., Durbin, R., et al. (2020). A haplotype-resolved, de novo genome assembly for the wood tiger moth (*Arctia plantaginis*) through trio binning. GigaScience **9**ARTN giaa088.10.1093/gigascience/giaa088.

Younis, A., Ramzan, F., Hwang, Y.J., and Lim, K.B. (2015). FISH and GISH: molecular cytogenetic tools and their applications in ornamental plants. Plant Cell Reports **34**:1477-1488. 10.1007/s00299-015-1828-3.

Zhang, T., Liu, G.Q., Zhao, H.N., Braz, G.T., and Jiang, J.M. (2021a). Chorus2: design of genome-scale oligonucleotide-based probes for fluorescence *in situ* hybridization. Plant Biotechnology Journal 10.1111/pbi.13610.

Zhang, Y.X., Zhang, G.Q., Zhang, D.Y., Liu, X.D., Xu, X.Y., Sun, W.H., Yu, X., Zhu, X.E., Wang, Z.W., Zhao, X., et al. (2021b). Chromosome-scale assembly of the *Dendrobium chrysotoxum* genome enhances the understanding of orchid evolution. Hortic Res-England **8**ARTN 183.10.1038/s41438-021-00621-z.

FIGURE LEGENDS

Figure 1. Endoreplicated and non-endoreplicated fractions in the CR0040 *Vanilla planifolia* genome. A. The histogram represents the distribution of nuclei in *V. planifolia* nodal tissues according to the strict partial endoreplication state of cells, from 2C (green), to 4E (blue), 8E (yellow), 16E (orange) and 32E (grey). The disks below represent the endoreplicated (coloured) and non-endoreplicated (black) DNA content for each class of nuclei, proportionally to their mass (pg). The lower cases f and p denote the respective DNA quantities of F (fixed proportion of the haploid genome which cannot endoreplicate) and P (part participating in endoreplication) fractions. The mean and the standard deviation (sd) of interpeak ratio has been indicated below the dotted arrows. **B.** F and P fractions and P/F ratio values obtained by flow cytometry, and detailed for P fraction for each nuclear class (2C, green; 4E, blue; 8E, yellow, 16E, orange and 32E, grey). **C.** Theoretical F and P fractions expected from HiFi sequencing and from flow cytometry obtained data. **D.** Theoretical (dotted) and experimental k-mer coverages for F (black) and P (hatched) fractions.

Figure 2. Cytogenetic analysis of *Vanilla planifolia* CR0040. **A-D.** Orcein staining: **A.** and **B.** Mitotic metaphases with 2n=32 chromosomes; **C.** Karyotype corresponding to figure B; **D.** Hypoaneuploid mitotic metaphase with 2n=28 chromosomes; **E.** Karyotype corresponding to figure D; **F.** Interphase nuclei showing heterochromatic chromocenters; **G.** DAPI stained interphase nucleus showing unspecific heterochromatin; **H.** Chromomycin fluorochrome staining with two CMA^+ regions (arrows) corresponding to rDNA sites; **I.** Hoechst stained AT-rich DNA in metaphase and interphase nucleus (IN), with two fully heterochromatinized chromosomes (arrows). Bar = 10 µm.

Figure 3. Assemblies k-mers content comparison between CR0040 PacBio HiFi long reads and Daphna Illumina short reads using spectra-cn graph. X-axis represents k-mers multiplicity (counts) and Y-axis the number of distinct k-mers multiplied by their counts. Because of different sequencing depths between read sets, the Y-axis upper values are 10^9 for figures **A** and **B** and 10^8 for figures **C** and **D**. The area colors indicate the number of k-mer copies (black: 0x or missing k-mers, red:1x, purple: 2x, green: 3x, blue: 4x and orange: 5x) found in the assembly. Four spectra-cn plots are presented: **A.** Daphna reads *vs* CR0040 assembly, **B.** Daphna reads *vs* Daphna assembly, **C.** CR0040 reads *vs* CR0040 assembly and **D.** CR0040 reads *vs* Daphna assembly. The red arrows point towards a low coverage k-mer distribution not expected in a diploid genome assembly spectra-cn graph. The black arrows

point towards the heterozygous (on the left) and homozygous (on the right) k-mer distributions expected in a diploïd genome assembly. The orange arrows point towards missing k-mers in the heterozygous k-mer distribution. The lower the black distribution at this location the less k-mers are missing in the assembly.

Figure 4. Overview of the assembled vanilla genome. A. Circos-plot of the genomic content along *V. planifolia* haplotypes A and B and the relationship between them. All tracks are divided in 500Kb genomic windows. From the outside to the inside of the circular representation: ideograms of 28 chromosomes and 2 random mosaic chromosomes that contain the unanchored scaffolds. Gene density (blue), interspersed repeats RepeatMasker hits density (black: retroelements; orange: LTR/Copia ; purple : LTR/Gypsy). Sequencing depth obtained by mapping CR0040 PacBio Hifi reads on the assembly (green) and N density (grey). Syntenic blocks across haplotypes are connected by lines in the innermost part of the figure. **B.** Sequencing depth along the CR0040 A03 and B03 chromosomes (red rectangles) obtained by mapping Daphna Illumina (yellow) and ONT (pink) reads, CR0040 PacBio Hifi (blue), Nanopore (green) and Illumina (grey) reads on the CR0040 assembly. Synteny between homologous chromosomes are represented by red boxes. Gaps (N stretches) explaining sudden drops in sequencing depth are shown with white blocks. (1) Low level of sequencing depth for all data. (2) Inverted level of sequencing depth for CR0040 between haplotypes A and B, and constant level of sequencing depth for both Daphna haplotypes. Gene and retrotransposons distributions along the chromosomes are represented by a blue line chart and a stacked histogram (copia: red, gypsy: purple, other retrotransposons: black) respectively.

Figure 5. Ratio of k-mers within unanchored and anchored CR0040 genome. This boxplot shows the ratio of k-mers with a depth below 15 in our HiFi reads, within unanchored sequences (blue) and within chromosomes (orange).

Figure 6. Overview (screen shots) of some interoperable vanilla genome analysis tools integrated into the vanilla genome hub. A. Main menu, **B.** Gene search (Tripal Megasearch), **C.** Sequence homology search (Blast), **D.** Gene report (Tripal), **E.** Genome Browser (JBrowse), **F.** Metabolic pathway visualization (Pathways Tools), **G.** GO Enrichment (DIANE), **H.** Comparison of genomic sequences (Synvisio).

TABLE

Table 1. HiFi assembly and annotation statistics of the diploid CR0040 genome.

Total assembly size (Gb)	3.4
Total contig number	24,534
Contig N50 length (Mb)	0.924
Maximum contig length (Mb)	31
GC content (%)	31.6
Number of protein coding genes	59,128
BUSCO completeness (%)	93.2
Total of interspersed repeats (%)	47.0

•

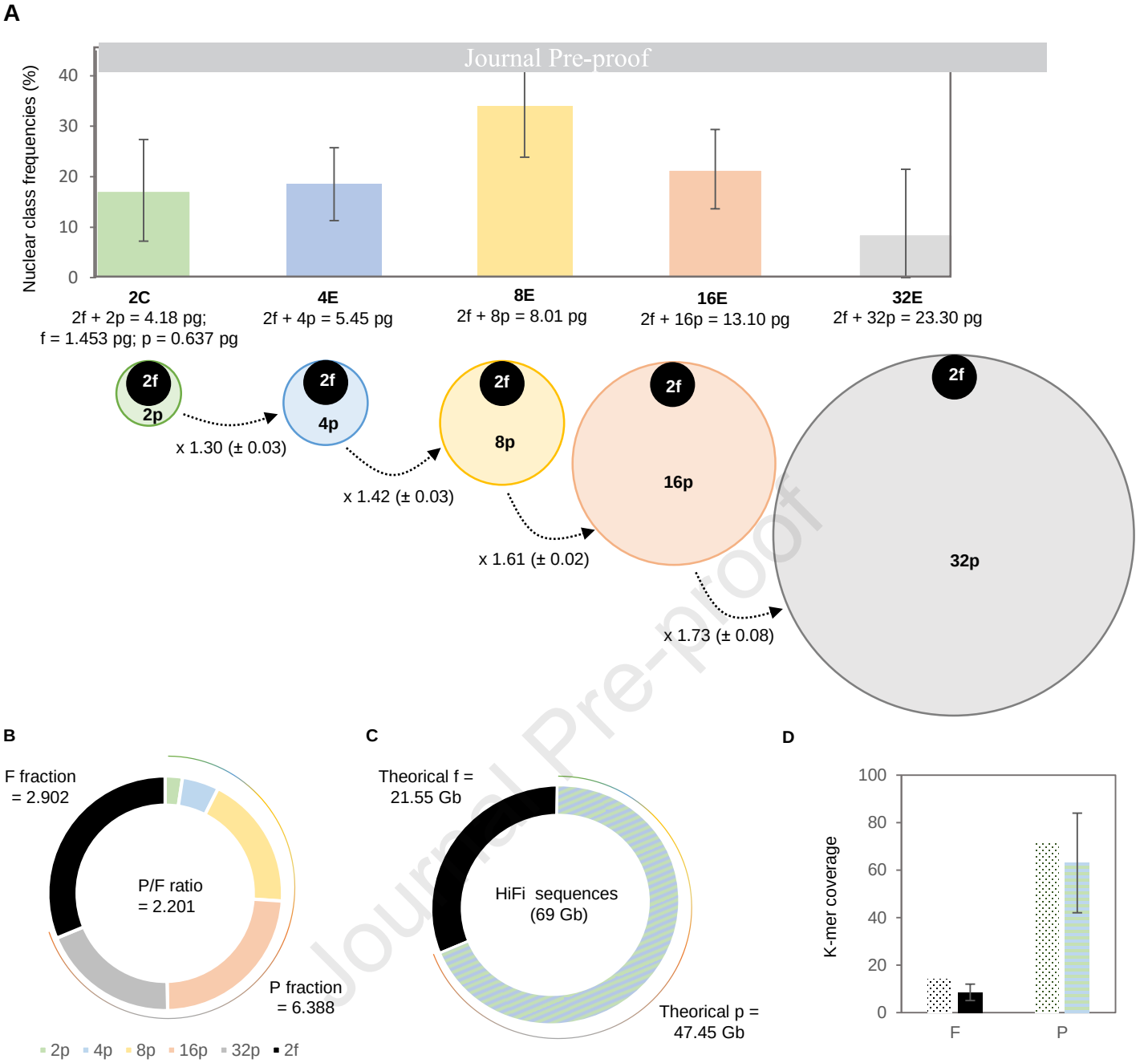

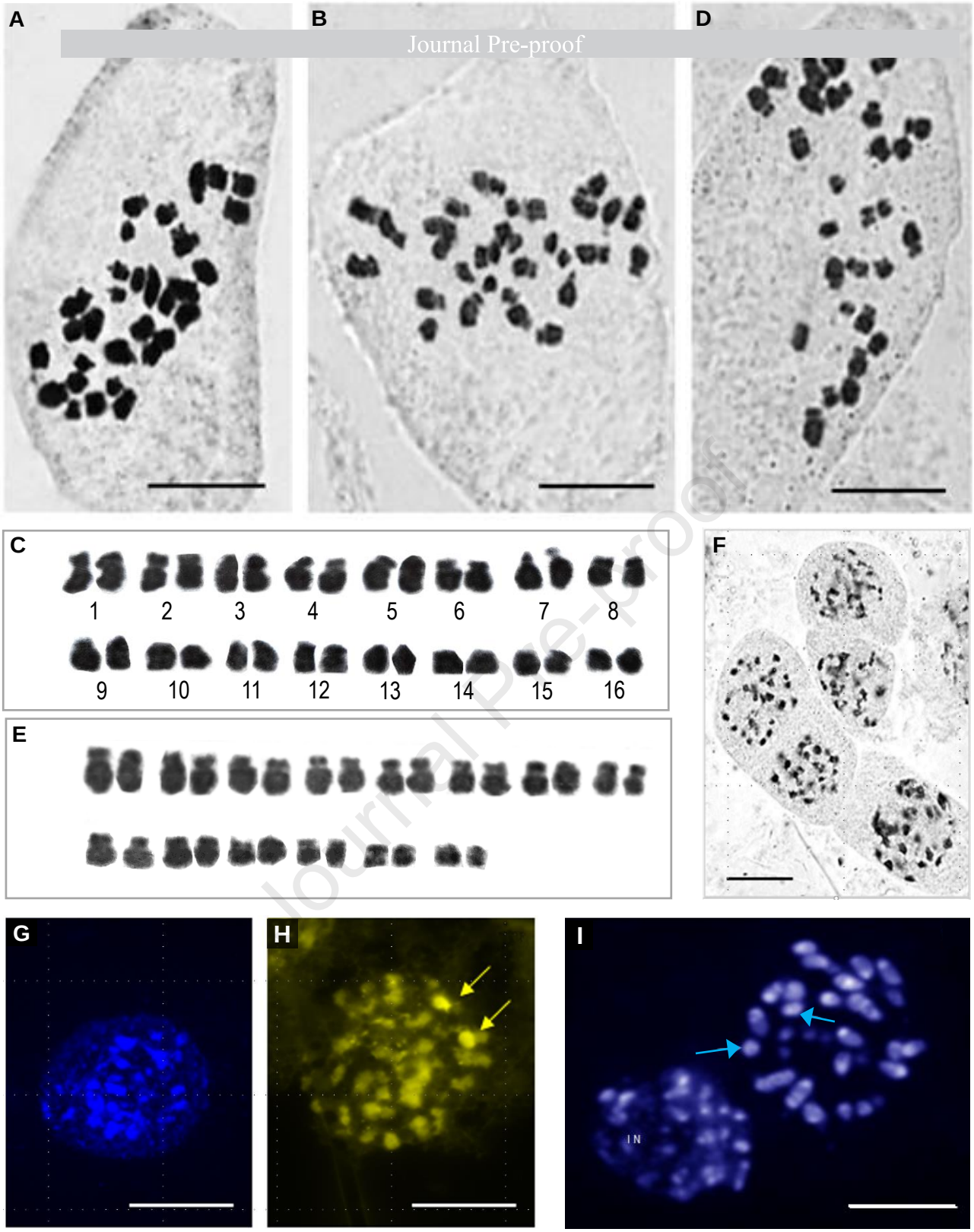

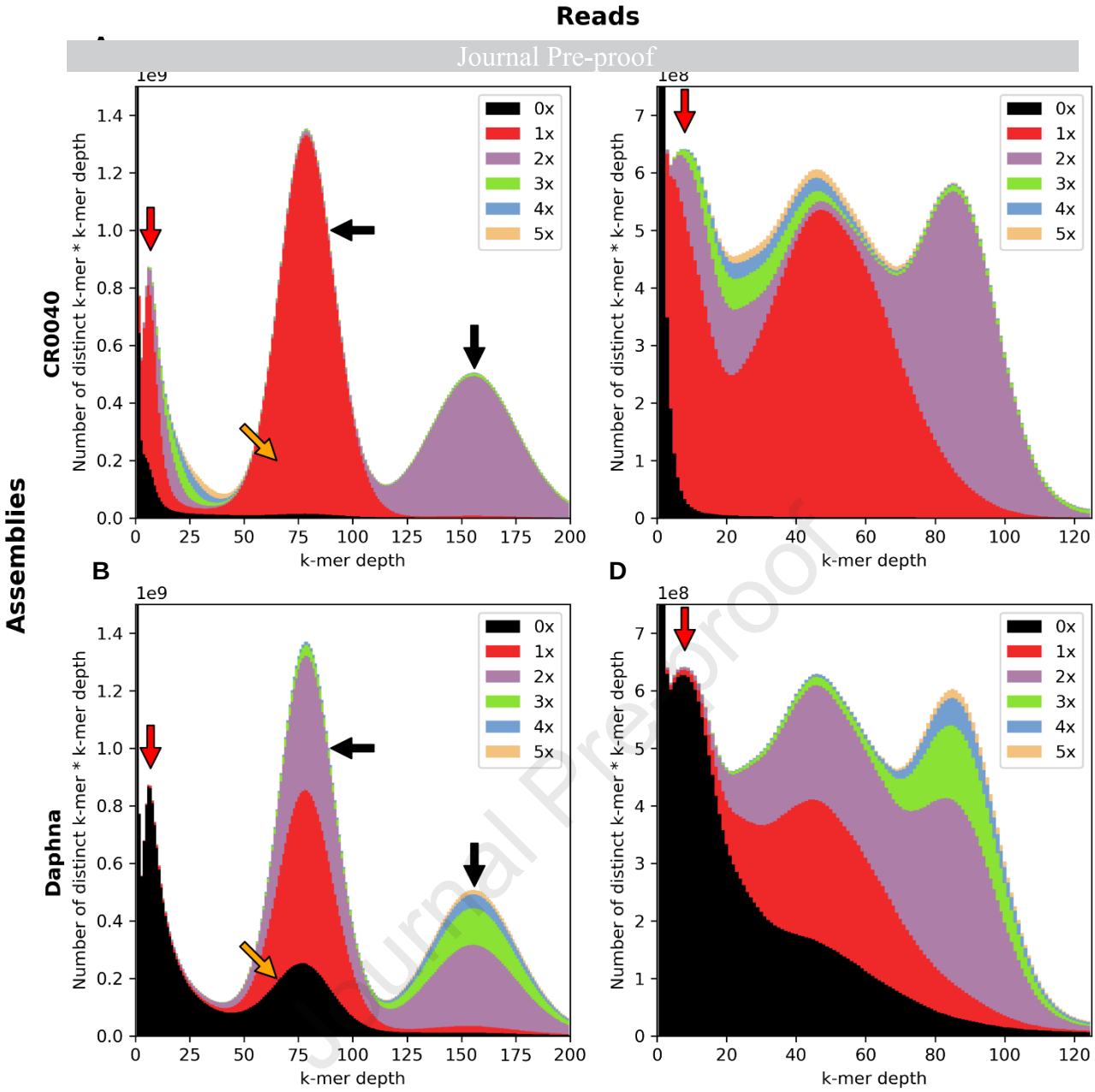

A

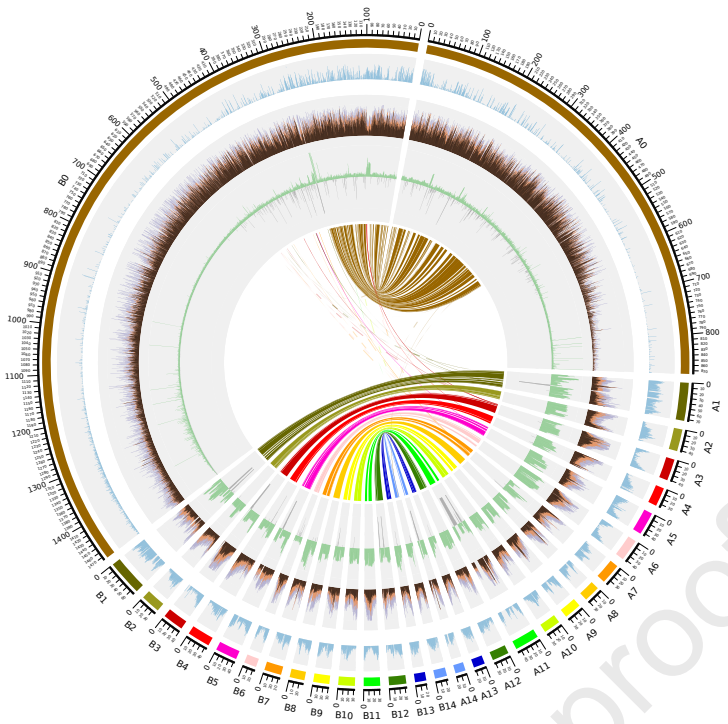

B